Tuning lipid structure by bile salts: hexosomes for topical administration of catechin

DOI: 10.1016/j.colsurfb.2021.111564

Marco Fornasier,[1,2,3,] Rosa Pireddu,[4] Alessandra Del Giudice,[5] Chiara Sinico,[4] Tommy Nylander,[3] Karin Schillén,[3] Luciano Galantini,[5] Sergio Murgia[1,2,*]*

[1]*Department of Chemical and Geological Sciences, University of Cagliari, s.s 554 bivio Sestu, Monserrato I-09042, Italy*

[2]*CSGI, Consorzio Interuniversitario per lo Sviluppo dei Sistemi a Grande Interfase, via della Lastruccia 3 Sesto Fiorentino, Florence, I-50019, Italy*

[3]*Division of Physical Chemistry, Department of Chemistry, Lund University, P.O. Box 124, Lund, SE-221 00, Sweden*

[4]*Department of Life and Environmental Sciences, University of Cagliari, via Ospedale 72, Cagliari I-09124, Italy*

[5]*Department of Chemistry, Sapienza University of Rome, P.le A. Moro 5, Rome 00185, Italy*

Corresponding authors:

Marco Fornasier (mfornasier@unica.it)

Sergio Murgia (murgias@unica.it)

Statistical summary of the article:

Number of words: 5996 (without references)

Number of Figures: 5

Number of Tables: 3

Abstract

The delivery of bio-active molecules through the skin is challenging given the complex structure of its outer layer, the *stratum corneum*. Here we explore the possibility to encapsulate bio-active compounds into nanocarriers containing permeation enhancers that can affect the fluidity of the *stratum corneum* lipids. This approach is expected to facilitate dermal or transdermal release. For this purpose, the application of bile salts, which are natural surfactants involved *in vivo* in lipid digestion, was exploited.

Bile salts were added to lipid liquid crystalline nanoparticles (NPs) made of monoolein for antioxidant topical delivery. Monoolein self-assembly behaviour in water was affected by the presence of bile salts molecules, giving a transition from a bicontinuous cubic to unilamellar vesicles dispersion. By adding oleic acid (OA), the change of curvature in the system led to a reverse hexagonal phase. The morphology, structure and size of the nanocarriers was investigated before the nanoparticles were loaded with catechin, a natural antioxidant occurring in plants and food. The encapsulation did not affect significantly the formulation phase behaviour. The formulation loaded with bile salts and catechin was thereafter tested *in vitro* on the skin from new-born pig. The results for two different lipid formulations without bile salts were compared under the same experimental conditions and with the same antioxidant. The formulation with bile salts showed the best performance, allowing a superior permeation of catechin in the different skin layers in comparison with formulations without bile salt.

Keywords: reverse hexagonal phase; skin; lipid liquid crystalline nanoparticles; natural antioxidants; mesophases; bile salts

1. Introduction

The skin represents an effective barrier for many organisms, preventing invasion of pathogens and regulating both water content and temperature.[1,2] It consists of several anatomically distinct layers, of which the *stratum corneum* (SC) is the external one. The SC is formed by corneocytes (protein-enriched anucleate cells) and lipid lamellar sheets.[3,4] This architecture, described by P. Elias as the 'bricks and mortar' model,[5] strongly restricts the diffusion of drugs and active compounds across the SC, limiting the efficacy of topical delivery of these molecules.[6]

Topical formulations containing permeation enhancers are applied to overcome this obstacle: they are able to make the SC more fluid and hence facilitate penetration of the drug.[7] Efficient carriers engineered for the dermal and transdermal release of active components include lipid dispersions such as liposomes,[2,8] ethosomes (phospholipids nanocarriers with a relative high concentration of ethanol)[9,10] and niosomes (non-ionic surfactant-based vesicles)[11–14]. However, most of these carriers have some limitations in terms of drug loading.[2]

Many life science applications exploit self-assembly of surfactants and lipids in water. The structure of these aggregates can be tuned by several parameters (i.e. temperature, concentration and composition in terms of salt, pH and additives). The particular type of structure formed can be rationalized by using the concept of the critical packing parameter (CPP). It is defined as the ratio between the volume of the hydrophobic tail of the surfactant (v), and the product of the surface area of the headgroup (a) times the length of the hydrophobic tail (l), i.e CPP = v/al.[15] For values of the packing parameter below 1, direct phases can be formed in water. As it approaches to 1, the lamellar phase become more favorable, whereas reverse phases can be obtained for values higher than 1. Among the latter, the reverse cubic bicontinuous and reverse hexagonal bulk phases can be dispersed in water to obtain non-lamellar liquid crystalline nanoparticles, called cubosomes and hexosomes,

respectively.[16,17] They possess a larger hydrophobic volume than their lamellar counterparts (i.e. liposomes) of the same size.[18] Herein, hexosomes and cubosomes will be discussed. In the reverse hexagonal phase, a lipid monolayer is curved towards water cylinders organized in a 2-dimensional hexagonal array. In the bicontinuous cubic phase, a curved lipid bilayer is formed in 3 dimensions in such a way that two systems of unconnected water channels are formed, with continuous regions of both water and lipid. The structure formed can be described as an infinite periodic minimal surface.[18] Both cubosomes and hexosomes can be formulated from different lipids, but monoolein-based aggregates are the most used for medical applications, given their low cytotoxicity.[18–20] Monoolein (or glycerol mono-oleate, GMO) forms a reverse hexagonal phase in water above 80 °C, depending on the purity of the sample.[21] Therefore, to favour the cubic bicontinuous-to-reverse hexagonal transition at room temperature, which is needed to formulate hexosomes, lipids such as oleic acid are needed as additives to increase the effective packing parameter.

Both hexosome and cubosome require adding a stabilizing agent to ensure their colloidal stability and avoid aggregation, and amphiphilic non-ionic tri-block copolymers of poly(ethylene oxide) (PEO) and poly(propylene oxide) (PPO), known as poloxamers, are used as the most common stabilizers.[18,22] The hydrophobic PPO middle block is partly buried in the lipid bilayer, whereas the two PEOs hydrophilic end blocks build up a corona surrounding the NP. This corona ensures sterical repulsive forces preventing the aggregation of the dispersed NPs.

Indeed, other kinds of stabilizers can be adopted, such as polyphosphoesters,[23] brush copolymers,[24] and polysorbate 80.[25] Recently, few examples of cubosomes and hexosomes that remain stable in water without adding a stabilizer were reported.[26–28]

Several compounds can be added to a formulation to enhance its permeation properties.[7,29,30] Among them, bile salts (BSs) are promising candidates as they are natural

surfactants, essential for the lipid digestion *in vivo*. The behaviour of these compounds and some derivatives in several biomedicine relevant systems, such as mixtures containing ionic[31,32] and non-ionic block copolymers [33–37] and lipids,[38–40] has been extensively investigated. Moreover, BSs derivatives have been synthesized to obtain drug carries suitable for delivery in the gastrointestinal tract to enhance the drug bioavailability,[41] and as building blocks for supramolecular structures, such as tubules and scrolls[42,43] able to organize into supra-colloidal frameworks.[44,45] Their importance in topical applications has been proven,[2,46] as they are considered to be "edge activators", e.g., bilayer softening components,[47] and can confer elastic properties to lipid vesicles.[48] Indeed, the presence of an edge activator into the formulation can increase the penetration of drugs through the skin *strata*.[49–51]

To our knowledge, only one experimental investigation has been devoted to explain the effect of a mixture of two BSs (sodium cholate (C) and sodium deoxycholate (DC)) on the structure and morphology of GMO- and phytantriol-based cubosomes.[52] It was found that the bicontinuous cubic Pn3m and Im3m to the lamellar bulk phases and their dispersions (cubosomes and vesicles, respectively) could be formed depending on the concentration and type of BS. However, the topical application of BSs-loaded non-lamellar lipid liquid crystalline dispersions has not yet been explored.

Among the bio-active compounds adopted for topical delivery, natural antioxidants have been widely studied due to their exceptional versatility. Catechin (Cat) is a natural polyphenol, found in several nutritional products. In the last decades, its beneficial properties as antiaging, antidiabetic, antibacterial, neuroprotective, and anti-inflammatory were reported.[53–55] Moreover, some studies highlighted that Cat has significant skin-photoprotection effect against UV-mediated oxidative stress and sunburns.[56] The application of this antioxidant is challenging due to short half-life *in vivo* and poor bioavailability after oral administration.[57]

Therefore, Cat was encapsulated in drug carriers suitable for dermal or transdermal release,[55,56,58,59] given that this administration route avoid the harsh environment of the gastrointestinal tract.

The effect of three different BSs, sodium cholate, sodium deoxycholate and sodium taurocholate (TC), on the structure and morphology of GMO-based liquid crystalline nanoparticles have been investigated with the prospect of applying these systems for the topical delivery of Cat. The bile salts used were selected based on their variation of hydrophilicity. After an initial screening, the best formulation in terms of its colloidal stability was loaded with Cat and their antioxidant activity and penetration ability on skin from new-born pigs evaluated *in vitro*.

Materials and Methods

2.1 Materials

The building block for the dispersions, RYLO MG 19 PHARMA, glycerol monooleate, 98.1 % wt (GMO), was kindly provided by Danisco Ingredients (Bradrand, Denmark). The bile salts sodium cholate, sodium deoxycholate and sodium taurocholate, as well as catechin (HPLC quality, purity ≥ 97 %), Pluronic® F108 (here denoted PF108) and oleic acid (GC quality, purity ≥ 99.0 %) were purchased from Sigma Aldrich. Lauroylcholine chloride (LCh, Titration quality and purity > 98 %) was purchased from TCI (Germany). MilliQ water (MilliQ Corporation, Bedford, MA) was used for the preparation of the nanoparticles' solutions.

2.2 Loaded and unloaded NPs preparation

The lipid liquid crystalline nanoparticles were prepared by melting GMO with or without oleic acid at 40 °C and thereafter an aqueous solution containing the poloxamer stabilizer PF108 and the BSs was added as described previously.[18,22] The GMO-PF108-BS mixture was

thereafter sonicated using a tip sonicator equipped with a controller (Sonics Vibra Cells, both from Chemical Instruments AB, Sweden) for 4 minutes at 30 % of amplitude and then for 6 minutes at 40 %, using the pulse in mode ON for 1 s and in mode OFF for 1 s (5 minutes of total sonication time). After ultrasonication, a milky or bluish dispersion was obtained, depending on the concentration of BSs and OA. To prepare the carriers loaded with the natural antioxidant, Cat was first dispersed in the lipid phase before mixing with the PF108-BS solution. The formulations obtained were stored at 25 °C prior to use and characterized 48 hours after preparation. The GMO:PF108 weight ratio was kept at 11:1 and the amount of dispersed phase was 3.6 – 4.6 wt (%), depending on the amount of BSs and OA added to the formulation. A typical volume for the samples was 2 mL.

The samples of hexosomes without bile salt (used for the *in vitro* studies) were prepared in the same manner, while the vesicles without BSs required the use of LCh instead of PF108.

For detailed compositions of the samples, see the **Supplementary Material**.

2.3 Cryogenic transmission electron microscopy

The morphology of the formulations was analyzed by cryogenic transmission electron microscopy (cryo-TEM) at the National Center for High Resolution Electron Microscopy (nCHREM) at Lund University. The instrument used was a JEM-2200FS transmission electron microscope (JEOL), equipped with a field-emission electron source, a cryo-pole piece in the objective lens and an in-column energy filter (omega filter). The recording of zero-loss images was acquired at an acceleration voltage of 200 kV on a bottom-mounted TemCam-F416 camera (TVIPS) using SerialEM under low-dose conditions. Each sample with the lipid nanoparticle dispersions was prepared using an automatic plunge freezer system (Leica Em GP) in an environmental chamber at 25.0 °C and 90 % of relative humidity. A 4 μL droplet of the dispersions of vesicles or hexosomes was deposited on a lacey formvar carbon-coated grid

(Ted Pella), and the excess liquid was removed with filter paper after blotting. The grids were plunged into liquid ethane (around –183 °C) to ensure the rapid vitrification of the sample in its native state, and thereafter stored in liquid nitrogen (–196 °C). Before an imaging session, the grids were transferred into the microscope using a cryo-transfer tomography holder (Fischione, Model 2550).

2.4 Dynamic light scattering and electrophoretic mobility measurements

The apparent hydrodynamic diameter (D_h) and the zeta (ζ) potential of the particles in the formulation were estimated by DLS measurements and by measurements of the electrophoretic mobility of the particles using a ZetaSizer Nano ZS by Malvern Instruments (now part of Malvern Panalytical) at (25.0 ± 0.1) °C,[60] set in a backscattering geometry at a fixed scattering angle of 173°. The nanoparticle dispersions were diluted in water 1:50 and analysed in disposable cuvettes. The values of the intensity-weighted D_h and polydispersity index (PdI) were extracted from a second order Cumulant analysis. The parameters were collected from at least six independent measurements of 10 runs each.

The electrophoretic mobilities were collected at a fixed scattering angle of 17° using laser Doppler electrophoresis method with disposable folded capillary cells (DTS1070). ζ potentials values were estimated from electrophoretic mobility by using Smoluchowski's equation and stated as the average of three consecutive measurements on the same solution together with the estimated standard deviation (SD). Before the measurements, the samples were diluted by a factor of 1:50 in water.

2.5 Small angle X-ray scattering

Small angle X-ray scattering patterns of the formulation were acquired with a SAXSLab Ganesha instrument (JJ-Xray, Denmark), equipped with a 30 W Cu X-ray micro-source

(Xenocs, France) and a 2D 300 K Pilatus detector (Dectris, Switzerland). The measurements were performed with a pin-hole collimated beam with the detector positioned asymmetrically at a distance of 480 mm from the sample, to yield azimuthally averaged intensities as a function of the scattering vector (q) over the range 0.012 – 0.67 $Å^{-1}$. The magnitude of the scattering vector is defined by $q = (4\pi\sin\theta)/\lambda$, where λ equals to 1.54 Å, Cu Kα wavelength, and θ is half of the scattering angle. The q scale was calibrated using silver behenate ($CH_3–(CH_2)_{20}$-COOAg) as a standard.

Samples were loaded in 1.5 mm quartz capillary cells and placed in a thermostat stage at 25 °C, controlled using a Julabo T Controller CF41 (Julabo Labortechnik GmbH, Germany, and equilibrated for 1800 s before any SAXS measurements

The d spacing was obtained from the positions of the Bragg peaks detected in the patterns (q_{peak}) by the following expression:

$$d = \frac{2\pi}{q_{peak}} \qquad \text{(eq. 1)}$$

Then, the lattice parameter of the liquid crystalline phase structure, a, was calculated from eq. 2 and eq. 3 for the bicontinuous cubic and for the hexagonal phases, respectively.[61]

$$a = d \cdot \sqrt{h^2 + k^2 + l^2} \qquad \text{(eq. 2)}$$

$$a = d \cdot \frac{2}{\sqrt{3}}\sqrt{h^2 + k^2 + hk} \qquad \text{(eq. 3)}$$

Here, *h*, *k* and *l* are the Miller indexes that describe the crystalline planes of lattice. The lattice parameter was used to evaluate the water channel radius (r_w) of the bicontinuous cubic phase (eq. 4) or of the hexagonal phase (eq. 5):

$$r_w = (a - l) \cdot \sqrt{\frac{A_0}{-2\pi\chi}} \qquad \text{(eq. 4)}$$

$$r_w = a \cdot \sqrt{1 - \varphi_{lipid}} \cdot \left(\frac{\sqrt{3}}{2 \cdot \pi}\right)^{\frac{1}{2}} \qquad \text{(eq. 5)}$$

where χ and A_0 are, respectively, the Euler characteristic and the surface area of the IPMS geometry (Pn3m, $\chi = -2$, $A_0 = 1.919$), and l is the GMO hydrophobic chain length at 25 °C (17 Å). The volume fraction, φ_{lipid}, was calculated using the following equation (eq. 6), where the parameters w_{lipids}, d_{lipids}, w_{water} and d_{water} are the weight and density of the lipid mixture (GMO+OA) and water respectively:

$$\varphi_{lipid} = \frac{\frac{w_{lipids}}{d_{lipids}}}{\left(\frac{w_{lipids}}{d_{lipids}} + \frac{w_{water}}{d_{water}}\right)} \qquad \text{(eq. 6)}$$

The values of d_{lipids}= 0.941g cm^{-3} and d_{water} = 0.998 g cm^{-3} were used.

2.6 Encapsulation Efficiency

Although Cat is strongly hydrophobic and thus expected to partition mostly in the lipid matrix, the formulations were dialyzed to remove possible traces of the solubilized antioxidant in the aqueous phase. The samples containing Cat were loaded into a dialysis tubing cellulose

membrane (14 kDa MW cutoff, purchased from Sigma Aldrich) and dialysed again 2 L of water for 2 h (by replacing the water after 1 h) at room temperature.

The absorption spectra of Cat (with an absorption maximum at 281 nm) were acquired using a Win-Cary Varian UV-Vis double beam spectrophotometer in EtOH. The standard calibration curve method was exploited to evaluate the loading of the antioxidant into the formulations via linear regression analysis (R^2 = 0.9999). A portion of the lipid formulations loaded with Cat was dissolved in EtOH before and after dialysis and placed in quartz cuvettes (1 cm of optical path).

The encapsulation efficiency (EE %) of the carriers was calculated using the following equation:

$$EE\ \% = \frac{m_{Cat\ after\ dialysis}}{m_{Cat\ before\ dialysis}} \cdot 100 \qquad \text{(eq. 7)}$$

where $m_{Cat\ after\ dyalisis}$ and $m_{Cat\ before\ dialysis}$ represent the mass of Cat evaluated *via* UV-Vis spectroscopy in the samples after and before dialysis, respectively.

2.7 DPPH test

The antioxidant activity of Cat-loaded formulations was assessed by evaluating their ability to scavenge the stable radical 2,2-diphenyl-1-picrylhydrazyl (DPPH). DPPH (0.04 mg/mL) dissolved in methanol was mixed with an appropriate amount of formulation to yield final Cat concentrations in the range 0.01 – 0.1 mg/mL. Empty formulations were also tested as control. Moreover, a negative control was prepared by mixing 990 µL of DPPH solution with 10 µL of water. After 30 minutes of incubation in the dark at room temperature, the absorbance was read at 517 nm by a Synergy 4 multiplate reader (BioTek, Winooski, USA). The percent antioxidant activity was calculated according to eq. 8.

$$antioxidant\ activity\ (\%) = \frac{(ABS_{control} - ABS_{sample})}{ABS_{control}} \cdot 100 \qquad \text{(eq. 8)}$$

where $ABS_{control}$ and ABS_{sample} are the absorbance of the Cat methanolic solution (control) and of the different Cat-loaded carriers (sample).

2.8 In vitro penetration and permeation studies

The ability of BS-loaded formulations to modulate Cat penetration and/or permeation through the skin was evaluated using skin from new-born pigs and the results were compared with the corresponding reference sample without BS. The experiments were performed in Franz vertical cells, exhibiting a diffusion area of 0.785 cm^2. The skin of one-day-old Goland–Pietrain hybrid pigs (~1.2 kg), died of natural causes and provided by a local slaughterhouse, was excised and stored at −80 °C until the day of the experiment. Skin specimens (n = 6 per formulation) were pre-equilibrated with saline (NaCl 0.9 % w/v) at 25 °C, then put between the donor and the receptor compartments. The receptor was filled with 5.5 mL of saline solution (NaCl 0.9 w/v %), continuously stirred and thermostated at (37 ± 1) °C, to emulate *in vivo* conditions. Exactly 200 µL of each formulation were placed onto the skin surface. At regular intervals, up to 8 h, the receiving solution was entirely withdrawn, replaced with fresh saline to ensure sink conditions and analysed by HPLC for catechin content. After 8 h, the skin surface was gently washed with 1 mL of distilled water and then dried with filter paper. The stratum corneum was removed by stripping with adhesive tape Tesa® AG (Hamburg, Germany). Each piece of adhesive tape was firmly pressed on the skin surface and rapidly pulled off with one stroke. Epidermis was separated from dermis with a surgical scalpel. Skin *strata* were cut, placed each in a flask with methanol and sonicated for 2 min to extract the accumulated drug. The tape and tissue suspensions were filtered out and assayed for drug content by HPLC.

2.9 HPLC method

Cat content was quantified at 222 nm using a chromatograph Alliance 2690 (Waters, Italy). The column was a XSelect HSS T3 (3.5 μm, 4.6 × 100 mm, Waters). The mobile phase was a mixture of acetonitrile, water and acetic acid (40.845:59.15:0.005 v/v), delivered at a flow rate of 0.3 mL/min. A standard calibration curve (R^2 of 0.999) was built up by using working, standard solutions (0.01 – 0.1 mg/mL).

2.10 Statistical analysis of data

Results are expressed as the mean ± SD. Multiple comparisons of means (one-way ANOVA with post-hoc Tukey HSD test) were used to substantiate statistical differences between groups, while Student's t-test was used to compare two samples. Data analysis was carried out with the software package XLStatistic for Microsoft Excel. Significance was tested at 0.05 level of probability (p).

3. Results and discussion

3.1 Effect of BSs on the cubosomes dispersion in water

First, a screening was conducted in order to evaluate the effect of the bile salts C, DC and TC on the structure of the GMO-based liquid crystalline nanoparticles. Here, the results in relation to the differences in chemical structures of the BSs used in this study will be discussed (Fig. 1a). The BSs typical facial amphiphilic moiety emerges from the hydroxyl groups-decorated backbone of condensed rings, which allows the molecule to intercalate into lipid bilayers and eventually disrupt them during the digestion.[62]

DC and C possess the same substitution in R_4 (DC does not have a –OH group in position R_2), while TC presents a taurine derivative with a larger polar group ($–SO_3^-$). The number of hydroxyl groups and the conjugation with hydrophilic aminoacids determine the

hydrophobic/hydrophilic balance on BSs molecules, which decreases in the order deoxycholate > cholate > taurocholate.

The BSs were loaded into the NPs in the range 0 – 1 wt % of the dispersion, containing 3.6 – 4.6 wt % of dispersed phase. Then, the (internal) structure and the size (apparent hydrodynamic diameter) of the particles in the formulations were evaluated by SAXS and DLS, respectively.

a)

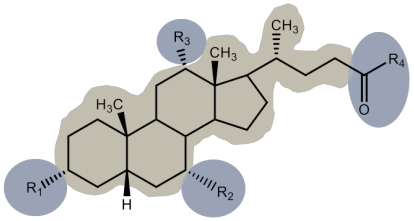

general structure of bile salts

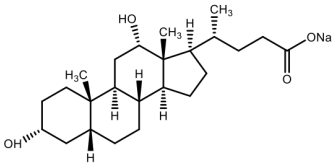

sodium deoxycholate (DC)

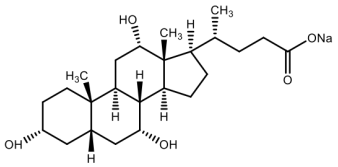

sodium cholate (C)

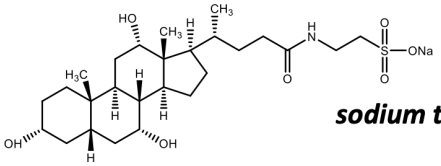

sodium taurocholate (TC)

b)

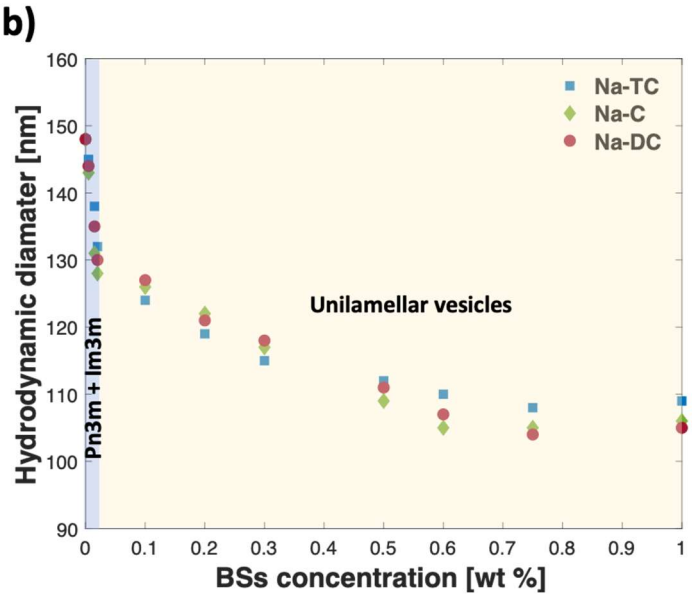

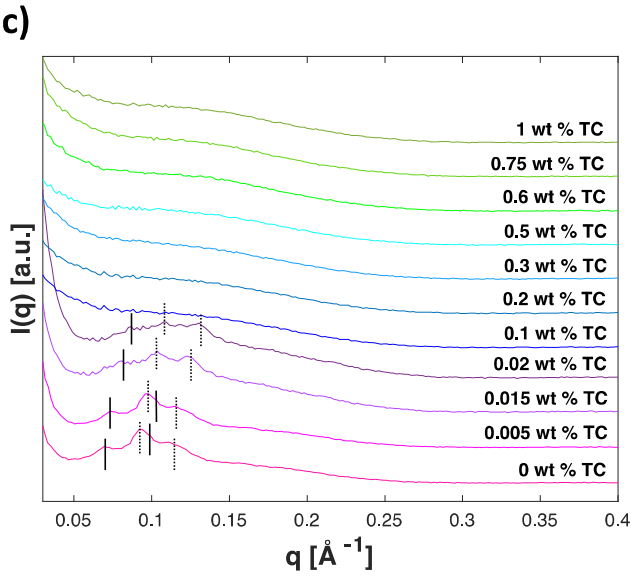

Figure 1. a) Chemical structure of the BSs used in the study. The steroid backbone (light yellow) is highly hydrophobic, while the different substituents (blue) define the hydrophilicity. The main difference between the three sodium bile salts is the substitution in R_4, equal to a taurine (-C=O-NH-CH_2-CH_2-SO_3^-) in the case of TC and a carboxylate (-COO^-) for both C and DC. Moreover, DC lacks a -OH in position R_2. b) The apparent hydrodynamic diameter by DLS is plotted against the BSs concentration (wt % of the dispersion). The errors in the measurements are less than 2 % for each point in the plot. The different structures inferred from SAXS results as a function of BSs content are highlighted as differently colored areas: light blue for the Pn3m + Im3m bicontinuous cubic phase and light green for unilamellar vesicles. c) SAXS patterns acquired for the formulations at 25 °C with increasing content of BSs. The lines on the peaks represent the Im3m (filled lines) and Pn3m (dashed lines) quasi-Bragg peaks. Even though only TC-loaded aggregates were reported in the plot, DC and C followed the same trend without any significant difference (data not shown).

The D_h values, upon addition of these BSs in the concentration range 0 – 1.0 wt %, to the formulation of cubosomes, suggest that the addition of bile salt reduces the size of the particles (Fig. 1b). Starting from a typical value of 148 nm for the cubosomes without BSs, no significant

effect on the size was observed up to a BS content of 0.015 wt %. By contrast, a remarkable decrease of the diameter was detected at larger BS concentration down to a plateau at D_h values of 107 – 110 nm, which was reached at around 0.6 wt % BS. Similar trends were observed for all of the investigated BSs, with no significant differences.

It is well known that GMO in excess water self-assembles into a bicontinuous cubic Pn3m phase. However, the presence of poloxamers, such as PF108, induces the formation of an additional bicontinuous cubic phase, the Im3m. This phenomenon was explained by Nakano as an interaction between the PPO moiety of the block copolymer and the GMO bilayer.[63] Indexing of the diffraction peaks from the SAXS pattern confirmed the coexistence of Pn3m and Im3m cubic phases in the copolymer-stabilized dispersion in the absence of BSs (Fig.1c). The two phases were preserved in the presence of small addition of BSs (< 0.02 wt %) to the formulation, although a slight decrease in the lattice parameters occurred since the diffraction peaks shifted to larger q values (see **Supplementary Material**). In parallel a decrease of the peak intensities was detected. A slight decrease in hydrodynamic diameter was also observed. A complete transition from reverse bicontinuous cubic phase to unilamellar vesicles took place above 0.02 wt % BS, as highlighted by the disappearance of the well resolved cubic diffraction that coincides with the appearance of a broad diffuse peak at larger q, related to the presence of vesicles (Fig.1c).

The observed strong effect of BSs on the GMO bilayers can be justified considering the capability of the bile salt molecules to intercalate the bilayer, leaving their charged heads in contact with the bulk water. This reduces the effective packing parameter and hence favours a phase transition from a reverse bicontinuous cubic to a lamellar phase.

We observed that, at the same BS concentration, the different BSs provided formulations with similar structure and size of the particles. However, a relevant effect of the BS type on the polydispersity of the formulations could be observed. In particular, the DC- and C-loaded

formulations exhibited higher PdI values (0.2 < PdI < 0.3) compared to the TC-loaded formulations (≤ 0.2). Moreover, a visual inspection revealed that both composition and BS type affected the stability of the formulations. Samples containing DC and C below 0.2 and above 0.5 wt % were destabilized after few days, whereas for BSs content between 0.2 and 0.5 wt % the samples lasted for two weeks on average. TC-loaded NPs remained stable for two months at TC content in the range 0.2 – 0.5 wt %, and 2 – 3 weeks at compositions outside this interval. According to the electrophoretic mobility measurements, DC- and C-loaded NPs presented an average ζ potential of (– 40 ± 2) mV while the NPs formulated with TC had (– 50 ± 1) mV. The higher (absolute value) ζ potential may explain the higher stability of the TC samples.

It deserves here noticing that, at least to a certain degree, the investigated BSs and PF108 may interact forming complexes, as already reported for different PEO-PPO-PEO block copolymers and another type of BS.[33,34,36] Therefore, a possible reason for the observed loss of colloidal stability when the BS concentration exceeds 0.5 wt % could be due to the reduced amount of PF108 available for the stabilization of the nanoparticles.

Among the stable formulations containing TC, the sample with composition GMO/TC/PF108/W = 3.3/0.3/0.3/96.1 (wt %) was selected for a more detailed characterization due to its stability at intermediate BS content. The morphology of the NPs was studied by cryo-TEM. In the micrographs spherical unilamellar vesicles were observed (Fig. 2a and b), corroborating the previous findings unveiled by SAXS.

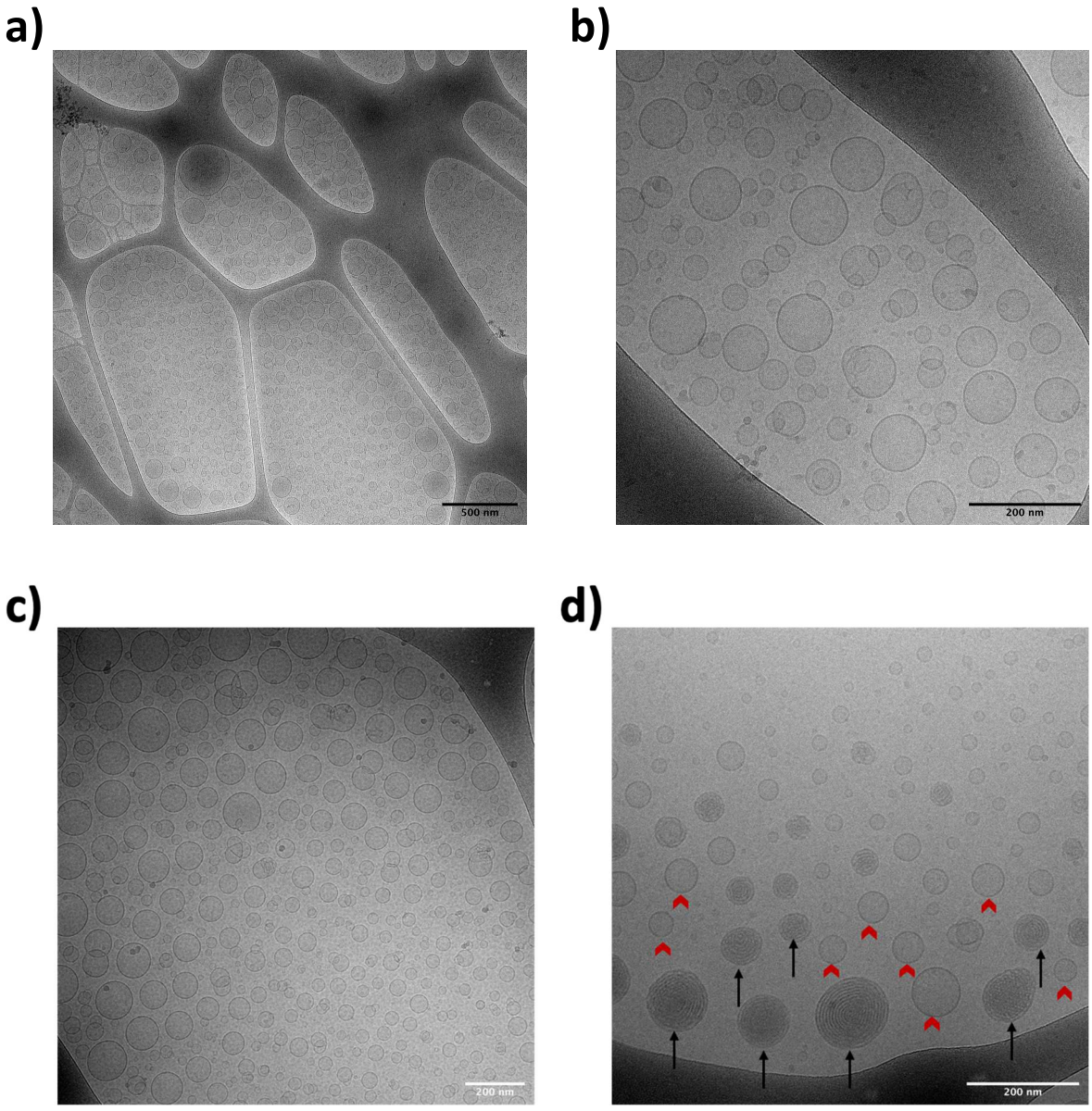

Figure 2. Cryo-TEM images of the formulations investigated. (a) and (b) GMO/TC/PF108/W = 3.3/0.3/0.3/96.1 (wt%) at a magnification of 15k and 60k, respectively. (c) GMO/OA/TC/PF108/W = 3.0/0.2/0.3/0.3/96.2, magnification of 30k. (d) GMO/OA/TC/PF108/W = 3.0/0.5/0.3/0.3/95.9 (wt%), at a magnification of 60k showing hexosomes (black arrows) and vesicles (red arrowheads).

3.2 Hexosomes containing bile salts

To create formulations based on hexosome dispersions, oleic acid was added to tune the interfacial curvature of the investigated systems. The effect of OA addition to the formulation containing TC was therefore explored in the OA concentration range 0.2 – 0.6 wt %. As revealed by cryo-TEM and SAXS experiments, vesicles were formed up to a content of 0.3 wt % OA, while hexosomes were obtained in the range 0.4 – 0.6 wt % of OA. Further addition of OA led to unstable formulations, undergoing complete macroscopic separation after few minutes. The morphology of the vesicles and hexosomes was studied by means of cryo-TEM (Fig. 2c and d).

Fig. 2c shows a typical micrograph of unilamellar vesicles. A few vesicles were interconnected or fused, highlighting the reduced curvature of the lipid bilayer induced by the presence of TC.[49] Increasing the OA concentration lead to the formation of hexosomes. This is evident from Fig. 2d, which shows a cryo-TEM image for a sample with composition GMO/OA/TC/PF108/W = 3.0/0.5/0.3/0.3/95.9 (wt%), that presents spherical and quasi-spherical particles with an inner-structure characterized by curved striations. These kind of morphologies are commonly reported in other studies of liquid crystalline nanoparticles with a reverse hexagonal phase.[64,65] The presence of unilamellar vesicles can also be discerned in the same micrograph (Fig. 2d).

SAXS patterns of the formulations with different OA concentrations are reported in Fig. 3.

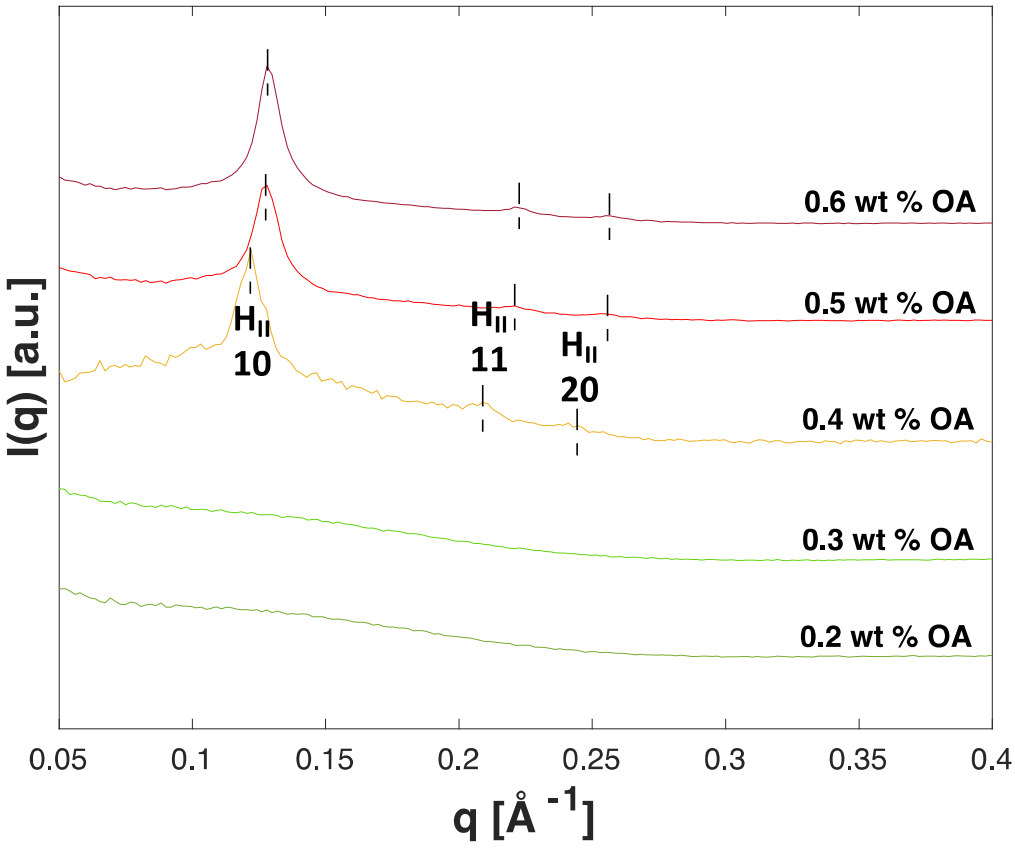

Figure 3. SAXS patterns of GMO/OA/TC/PF108/W systems with increasing concentration of OA at 25 °C. The ~~quasi-~~Bragg peaks related to the reverse hexagonal phase (H_{II}) are indicated by vertical black lines.

As already mentioned, increasing the OA concentration affected the self-assembly properties of GMO. At 0.2 wt % the amount of OA was not enough to counterbalance the lamellar-forming effect of TC and therefore the SAXS curve reflects a formulation containing only vesicles (Fig.3). At 0.4 wt % a lamellar-to-hexagonal phase transition phase was observed. The presence of the reverse hexagonal symmetry was proved by three peaks in the SAXS pattern positioned at q values in the ratio 1: $\sqrt{3}$: $\sqrt{4}$. The radius of the water channels calculated from the peak positions was observed to slightly decrease with OA addition (Table 1). Further increasing the amount of OA destabilized the system, with consequent phase separation.

The most stable hexagonal phase dispersion was the one containing 0.5 wt % of OA, which was stable for more than one month as judged by visual inspection.

Table 1. Effect of OA concentration on NPs structure. Composition is given in wt %. Lattice parameters and water channel radii were calculated from eq.3 and eq.5.

GMO/OA/TC/PF108/W	***Phase***	***a (Å)***	***r_w (Å)***
3.3/0.2/0.3/0.3/95.9	Vesicles	-	-
3.3/0.3/0.3/0.3/95.8	Vesicles	-	-
3.3/0.4/0.3/0.3/95.7	H_{II}	58.9 ± 0.2	30.4 ± 0.1
3.3/0.5/0.3/0.3/95.6	H_{II}	56.7 ± 0.2	29.2 ± 0.1
3.3/0.6/0.3/0.3/95.5	H_{II}	55.0 ± 0.1	28.4 ± 0.1

3.3 Encapsulation of catechin into hexosomes

Encapsulation of payloads into a lipid liquid crystalline phase represents an effective method to overcome the poor water solubility of several bio-actives. Here, the encapsulation of a natural antioxidant, Cat, into a non-lamellar lipid phase dispersion was studied to prepare NPs for topical application. Given the hydrophobic character of Cat, the antioxidant was effectively incapsulated into the reverse hexagonal phase of the formulation GMO/OA/TC/PF108/W = 3.0/0.5/0.3/0.3/95.9. This composition was chosen since it has an intermediate OA content among those samples that formed hexosomes. The Cat-loaded formulation (HexTC + Cat) was then compared with two blanks: TC-loaded hexosomes with the same composition (HexTC) and a classical hexosomes (Hex) dispersion (GMO/OA/PF108/W = 3.0/0.5/0.3/96.2) without the BS.

In comparison with the two blank samples, the Cat loading did not significantly affect the structure, size, polydispersity, and ζ potential, as shown in Figure 4 and Table 2.

Regarding the shelf-life of the formulation, the Cat-loaded NPs did not exhibit any phase separation for 1 month after checking the samples each week by visual inspection.

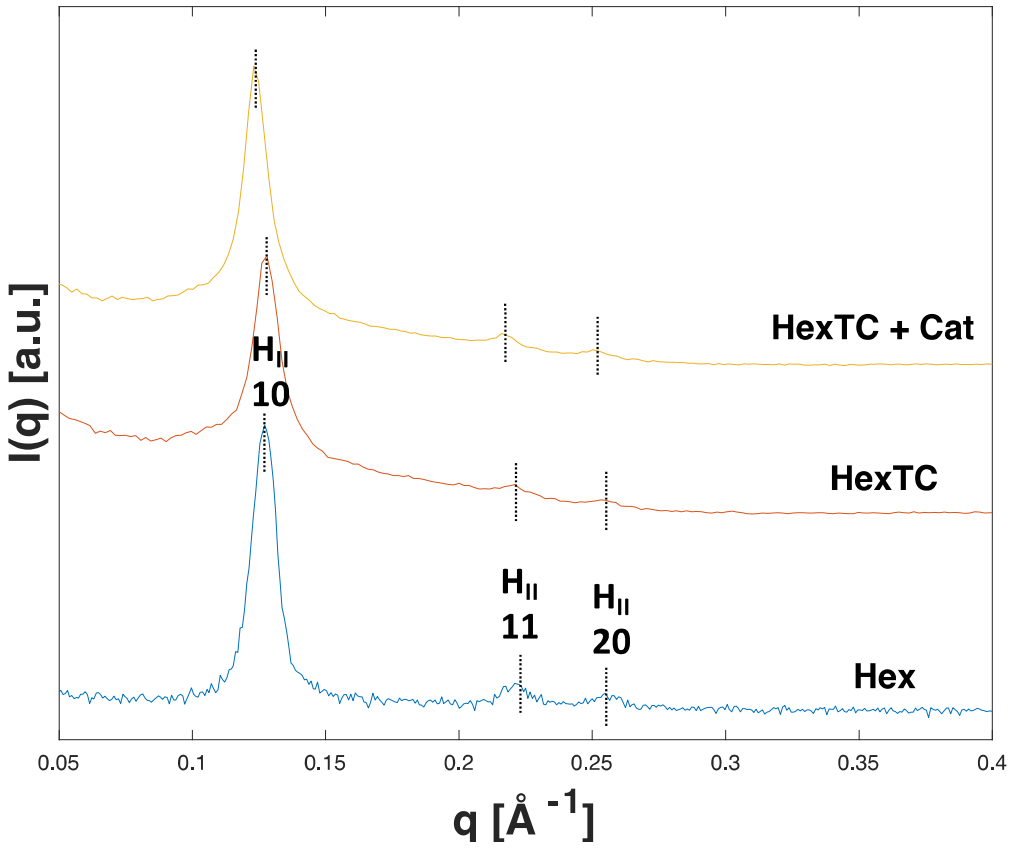

Figure 4. SAXS patterns of the formulation of hexosomes (Hex), TC-loaded hexosomes (HexTC) and TC-loaded hexosomes with catechin encapsulated (HexTC + Cat) at 25 °C.

Table 2. Lattice parameters (*a*), apparent hydrodynamic diameters (D_h), polydispersity index (PdI) and ζ potentials for the loaded and unloaded formulations evaluated by SAXS, DLS, and electrophoretic mobility measurements.

Sample	a (Å)	r_w (Å)	D_h (nm)	PdI	ζ (mV)
Hex	56.9 ± 0.2	29.3 ± 0.1	160 ± 2	0.10 ± 0.02	–30 ± 1

HexTC	56.7 ± 0.2	29.2 ± 0.1	157 ± 1	0.13 ± 0.01	–52 ± 1
HexTC + Cat	58.2 ± 0.7	30.0 ± 0.3	158 ± 1	0.14 ± 0.01	–54 ± 2

3.4 In vitro permeation study on skin from new-born pigs

Based on these results and aiming to a possible topical application of these new NPs, *in vitro* penetration and permeation tests were performed through new-born pig skin, using Franz diffusion cells under non-occlusive conditions.

The capacity of HexTC to deliver Cat into and through the skin during *in vitro* experiments was compared to that of both hexosomes without TC (Hex + Cat) and vesicles formed by GMO and lauroylcholine (Ves + Cat),[8,29,30] which were loaded with the same amount of antioxidant (see **Supplementary Material** for the SAXS patterns of the empty and Cat-loaded formulations without TC). In Table 4, the general information about these samples is reported.

Table 3. Parameters obtained from DLS, electrophoretic mobility and encapsulation efficiency measurements on the samples used in the *in vitro* study.

samples	**D_h (nm)**	**PdI**	**ζ (mV)**	**EE %**	**Cat Concentration (mg/mL)**
HexTC + Cat	158 ± 1	0.14 ± 0.01	–54 ± 2	99.9 ± 0.1	1.00 ± 0.1
Hex + Cat	160 ± 2	0.13 ± 0.01	–29 ± 1	99.5 ± 0.2	0.99 ± 0.1
Ves + Cat	80 ± 3	0.24 ± 0.01	+42 ± 2	97.4 ± 1.2	0.95 ± 0.5

Results from the (trans)dermal experiments are shown in Fig. 5a. As expected, based on previous studies,[8,30] after 8 h of treatment the GMO vesicles (Ves + Cat) increased the skin

Cat penetration and accumulation, particularly in the epidermis, as compared to both Hex formulations, while no transdermal release could be observed in the receptor fluids.

Conversely, although the cumulative amount of Cat accumulated in all the three skin layers was lower than that recovered after vesicles application, the conventional hexosomes (Hex) enhanced Cat permeation through the skin. Indeed, 1.15 % of the applied Cat dose was recovered in the receptor compartment after 2 hours experiment (data not shown), and 4.56 % after 8 h.

The formulation containing TC, i.e., HexTC, showed a significantly higher drug accumulation in the different skin layers compared to both Hex without TC and vesicles. Indeed, the Cat amount found in the stratum corneum was approximately three and two-fold higher than traditional Hex and vesicle formulations, respectively. Furthermore, also the accumulation in the deeper skin layers as well as the transdermal permeation increased as can be clearly noticed in Fig. 5a. These data suggest that the HexTC nanoparticles, thanks to the synergic action of the penetration enhancers GMO and OA and the edge activator TC, are able to facilitate the Cat penetration into the stratum corneum, where it creates a depot by which slowly diffuses through the skin layers.

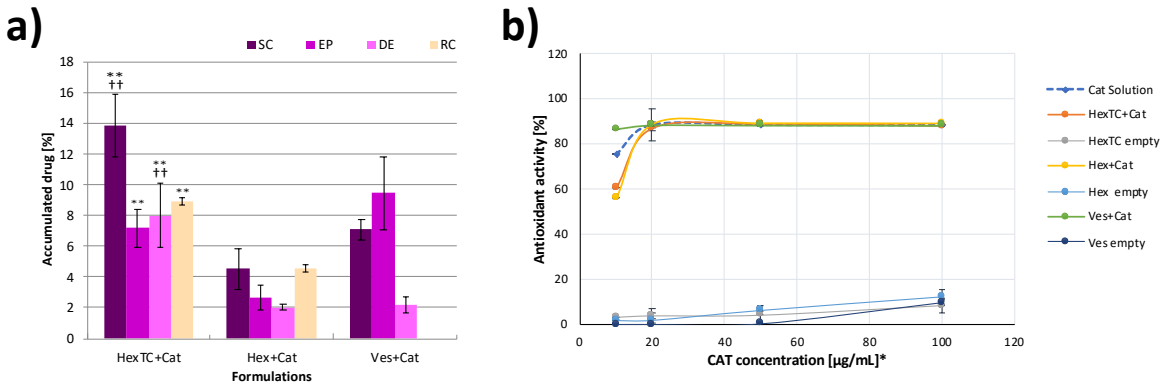

Figure 5. (a) Cumulative amount of Cat retained into and permeated through the skin layers after 8 h-treatment with TC-loaded hexosomes (HexTC + Cat), hexosomes without TC (Hex +

Cat) and a GMO-vesicle formulation (Ves + Cat). SC, Ep, D and RC denote stratum corneum, epidermis, dermis and receptor compartment, respectively. Results are reported as means ± SD of at least 6 independent determinations. Symbols represent significance of differences between HexTC and Hex, ** $P < 0.01$, and between HexTC and Ves, †† $P < 0.01$. (b) *In vitro* antioxidant activity of TC-loaded hexosomes (HexTC + Cat), hexosomes without TC (Hex + Cat) and a GMO-based vesicle formulation (Ves + Cat). Results are reported as the mean value ± SD of three separate experiments, each performed in triplicate. * Empty formulations were also tested as control at the same dilution of Cat loaded formulations.

3.5. In vitro antioxidant activity

Finally, to evaluate the effect of Cat encapsulation on its intrinsic antioxidant activity, a DPPH assay experiment was performed. Fig. 5b presents the antioxidant activity of the different Cat formulations expressed as % inhibition of the DPPH radical as compared to a Cat in methanol solution. In order to verify a possible antioxidant activity of the formulation components, the formulations without Cat were also tested. Results showed that in the range between 20 – 100 µg/mL of Cat concentration, all the tested formulations exert a high and statistically equivalent antioxidant activity with a DPPH radical inhibition of ~ 88 %. These outcomes demonstrate that Cat preserves its strong antioxidant activity after hexosome encapsulation, while the formulation components did not affect it.

4. Conclusions

Administration of drugs or bio-actives on skin represents a convenient and non-invasive therapeutic route, although it can be challenging to overcome the skin barrier, especially the *stratum corneum*. Previously, vesicles were widely studied for this task, formulated with

permeation enhancers and edge activators.[8,10,66–68] However, vesicular carriers have limitations in terms of cargo loading that restrict their therapeutical efficacy.[2,18]

In this work, we have shown that lipid-based NPs formulation for topical application containing permeation enhancers, such as GMO and OA, and edge activators (i.e., BSs) can tackle the challenges in terms of limited cargo loading and skin penetration. The effect of three bile salts of varying hydrophilicity, i.e., sodium cholate, sodium deoxycholate and sodium taurocholate were evaluated by using SAXS, DLS and cryo-TEM with the purpose of formulating the most stable composition. A natural antioxidant, catechin, was loaded into hexosomes. The *in vitro* penetration tests showed that the presence of BSs in the hexosomes enhances the penetration properties, favoring accumulation in the deeper skin layers and transdermal permeation in comparison with the hexosomes and vesicles without BSs. Moreover, DPPH test showed that the antioxidant properties of Cat were retained after encapsulation into the hexosomes.

As a future perspective, formulations of BS gels will be adopted to enhance its applicability compared to liquid formulations, for the reason that a gel is expected to be applied on the skin more easily than a liquid, and hence increase the efficacy of the therapy.

5. Acknowledgements

The authors thank Dr. Anna M. Carnerup for her kind assistance with the cryo-TEM measurements. SAXSLab Sapienza is kindly acknowledged for providing preliminary SAXS analyses. Ph.D. scholarship of M.F. was funded by the project P.O.R. Sardegna F.S.E. 2014-2020. S.M. thanks Fondazione Banco di Sardegna and Regione Autonoma della Sardegna (Progetti Biennali di Ateneo Annualità 2018).

References

[1] A. Wolde-Kidan, Q.D. Pham, A. Schlaich, P. Loche, E. Sparr, R.R. Netz, E. Schneck, Influence of polar co-solutes and salt on the hydration of lipid membranes, Phys. Chem. Chem. Phys. 21 (2019) 16989–17000. https://doi.org/10.1039/c9cp01953g.

[2] F. Lai, C. Caddeo, M.L. Manca, M. Manconi, C. Sinico, A.M. Fadda, What's new in the field of phospholipid vesicular nanocarriers for skin drug delivery, Int. J. Pharm. 583 (2020). https://doi.org/10.1016/j.ijpharm.2020.119398.

[3] M.L. González-Rodríguez, A.M. Rabasco, Charged liposomes as carriers to enhance the permeation through the skin, Expert Opin. Drug Deliv. 8 (2011) 857–871. https://doi.org/10.1517/17425247.2011.574610.

[4] S.M. Pyo, H.I. Maibach, Skin Metabolism: Relevance of Skin Enzymes for Rational Drug Design, Skin Pharmacol. Physiol. 32 (2019) 283–293. https://doi.org/10.1159/000501732.

[5] P.M. Elias, Structure and function of the stratum corneum extracellular matrix, J. Invest. Dermatol. 132 (2012) 2131–2133. https://doi.org/10.1038/jid.2012.246.

[6] S. Björklund, Q.D. Pham, L.B. Jensen, N.Ø. Knudsen, L.D. Nielsen, K. Ekelund, T. Ruzgas, J. Engblom, E. Sparr, The effects of polar excipients transcutol and dexpanthenol on molecular mobility, permeability, and electrical impedance of the skin barrier, J. Colloid Interface Sci. 479 (2016) 207–220. https://doi.org/10.1016/j.jcis.2016.06.054.

[7] Q.D. Pham, S. Björklund, J. Engblom, D. Topgaard, E. Sparr, Chemical penetration enhancers in stratum corneum - Relation between molecular effects and barrier function, J. Control. Release. 232 (2016) 175–187. https://doi.org/10.1016/j.jconrel.2016.04.030.

[8] M. Schlich, M. Fornasier, M. Nieddu, C. Sinico, S. Murgia, A. Rescigno, 3-

Hydroxycoumarin Loaded Vesicles for Recombinant Human Tyrosinase Inhibition in Topical Applications, Colloids Surfaces B Biointerfaces. 171 (2018) 675–681. https://doi.org/10.1016/j.colsurfb.2018.08.008.

[9] A. Mistry, P. Ravikumar, Development and evaluation of azelaic acid based ethosomes for topical delivery for the treatment of acne, Indian J. Pharm. Educ. Res. 50 (2016) S232–S243. https://doi.org/10.5530/ijper.50.3.34.

[10] G. Sharma, H. Goyal, K. Thakur, K. Raza, O.P. Katare, Novel elastic membrane vesicles (EMVs) and ethosomes-mediated effective topical delivery of aceclofenac: a new therapeutic approach for pain and inflammation, Drug Deliv. 23 (2016) 3135–3145. https://doi.org/10.3109/10717544.2016.1155244.

[11] M.L. Manca, M. Manconi, A. Nacher, C. Carbone, D. Valenti, A.M. MacCioni, C. Sinico, A.M. Fadda, Development of novel diolein-niosomes for cutaneous delivery of tretinoin: Influence of formulation and in vitro assessment, Int. J. Pharm. 477 (2014) 176–186. https://doi.org/10.1016/j.ijpharm.2014.10.031.

[12] S.R.M. Moghddam, A. Ahad, M. Aqil, S.S. Imam, Y. Sultana, Formulation and optimization of niosomes for topical diacerein delivery using 3-factor, 3-level Box-Behnken design for the management of psoriasis, Mater. Sci. Eng. C. 69 (2016) 789–797. https://doi.org/10.1016/j.msec.2016.07.043.

[13] L. Tavano, P. Alfano, R. Muzzalupo, B. De Cindio, Niosomes vs microemulsions: New carriers for topical delivery of Capsaicin, Colloids Surfaces B Biointerfaces. 87 (2011) 333–339. https://doi.org/10.1016/j.colsurfb.2011.05.041.

[14] M. Ravaghi, S.H. Razavi, S.M. Mousavi, C. Sinico, A.M. Fadda, Stabilization of natural canthaxanthin produced by Dietzia natronolimnaea HS-1 by encapsulation in niosomes, LWT - Food Sci. Technol. 73 (2016) 498–504. https://doi.org/10.1016/j.lwt.2016.06.027.

[15] J.N. Israelachvili, D.J. Mitchell, B.W. Ninham, Theory of self-assembly of hydrocarbon amphiphiles into micelles and bilayers, J. Chem. Soc. Faraday Trans. 2 Mol. Chem. Phys. (1976). https://doi.org/10.1039/F29767201525.

[16] J. Gustafsson, H. Ljusberg-Wahren, M. Almgren, K. Larsson, Submicron particles of reversed lipid phases in water stabilized by a nonionic amphiphilic polymer, Langmuir. 13 (1997) 6964–6971. https://doi.org/10.1021/la970566+.

[17] C. Neto, G. Aloisi, P. Baglioni, K. Larsson, Imaging soft matter with the atomic force microscope: Cubosomes and hexosomes, J. Phys. Chem. B. (1999). https://doi.org/10.1021/jp984551b.

[18] S. Murgia, S. Biffi, R. Mezzenga, Recent advances of non-lamellar lyotropic liquid crystalline nanoparticles in nanomedicine, Curr. Opin. Colloid Interface Sci. 48 (2020) 28–39. https://doi.org/10.1016/j.cocis.2020.03.006.

[19] S. Biffi, L. Andolfi, C. Caltagirone, C. Garrovo, A.M. Falchi, V. Lippolis, A. Lorenzon, P. Macor, V. Meli, M. Monduzzi, M. Obiols-Rabasa, L. Petrizza, L. Prodi, A. Rosa, J. Schmidt, Y. Talmon, S. Murgia, Cubosomes for in vivo fluorescence lifetime imaging, Nanotechnology. 28 (2017). https://doi.org/10.1088/1361-6528/28/5/055102.

[20] V. Meli, C. Caltagirone, A.M. Falchi, S.T. Hyde, V. Lippolis, M. Monduzzi, M. Obiols-Rabasa, A. Rosa, J. Schmidt, Y. Talmon, S. Murgia, Docetaxel-Loaded Fluorescent Liquid-Crystalline Nanoparticles for Cancer Theranostics, Langmuir. 31 (2015) 9566–9575. https://doi.org/10.1021/acs.langmuir.5b02101.

[21] H. Qiu, M. Caffrey, The phase diagram of the monoolein/water system: Metastability and equilibrium aspects, Biomaterials. 21 (2000) 223–234. https://doi.org/10.1016/S0142-9612(99)00126-X.

[22] H.M.G. Barriga, M.N. Holme, M.M. Stevens, Cubosomes: The Next Generation of

Smart Lipid Nanoparticles?, Angew. Chemie - Int. Ed. 58 (2019) 2958–2978. https://doi.org/10.1002/anie.201804067.

[23] M. Fornasier, S. Biffi, B. Bortot, P. Macor, A. Manhart, F.R. Wurm, S. Murgia, Cubosomes stabilized by a polyphosphoester-analog of Pluronic F127 with reduced cytotoxicity, J. Colloid Interface Sci. 580 (2020) 286–297. https://doi.org/10.1016/j.jcis.2020.07.038.

[24] J.Y.T. Chong, X. Mulet, A. Postma, D.J. Keddie, L.J. Waddington, B.J. Boyd, C.J. Drummond, Novel RAFT amphiphilic brush copolymer steric stabilisers for cubosomes: Poly(octadecyl acrylate)-block-poly(polyethylene glycol methyl ether acrylate), Soft Matter. 10 (2014) 6666–6676. https://doi.org/10.1039/c4sm01064g.

[25] M. Valldeperas, A.P. Dabkowska, G.K. Pálsson, S. Rogers, N. Mahmoudi, A. Carnerup, J. Barauskas, T. Nylander, Interfacial properties of lipid sponge-like nanoparticles and the role of stabilizer on particle structure and surface interactions, Soft Matter. 15 (2019) 2178–2189. https://doi.org/10.1039/c8sm02634c.

[26] U. Bazylińska, J. Kulbacka, J. Schmidt, Y. Talmon, S. Murgia, Polymer-free cubosomes for simultaneous bioimaging and photodynamic action of photosensitizers in melanoma skin cancer cells, J. Colloid Interface Sci. 522 (2018) 163–173. https://doi.org/10.1016/j.jcis.2018.03.063.

[27] F. Muller, A. Salonen, O. Glatter, Phase behavior of Phytantriol/water bicontinuous cubic Pn3m cubosomes stabilized by Laponite disc-like particles, J. Colloid Interface Sci. 342 (2010) 392–398. https://doi.org/10.1016/j.jcis.2009.10.054.

[28] J. Zhai, L. Waddington, T.J. Wooster, M.I. Aguilar, B.J. Boyd, Revisiting β-casein as a stabilizer for lipid liquid crystalline nanostructured particles, Langmuir. 27 (2011) 14757–14766. https://doi.org/10.1021/la203061f.

[29] R. Angelico, M. Carboni, S. Lampis, J. Schmidt, Y. Talmon, M. Monduzzi, S. Murgia,

Physicochemical and rheological properties of a novel monoolein-based vesicle gel, Soft Matter. 9 (2013) 921–928. https://doi.org/10.1039/c2sm27215f.

[30] M. Carboni, A.M. Falchi, S. Lampis, C. Sinico, M.L. Manca, J. Schmidt, Y. Talmon, S. Murgia, M. Monduzzi, Physicochemical, Cytotoxic, and Dermal Release Features of a Novel Cationic Liposome Nanocarrier, Adv. Healthc. Mater. (2013). https://doi.org/10.1002/adhm.201200302.

[31] K. Schillén, L. Galantini, G. Du, A. Del Giudice, V. Alfredsson, A.M. Carnerup, N. V. Pavel, G. Masci, B. Nyström, Block copolymers as bile salt sequestrants: Intriguing structures formed in a mixture of an oppositely charged amphiphilic block copolymer and bile salt, Phys. Chem. Chem. Phys. 21 (2019) 12518–12529. https://doi.org/10.1039/c9cp01744e.

[32] M.C. Di Gregorio, M. Gubitosi, L. Travaglini, N. V. Pavel, A. Jover, F. Meijide, J. Vázquez Tato, S. Sennato, K. Schillén, F. Tranchini, S. De Santis, G. Masci, L. Galantini, Supramolecular assembly of a thermoresponsive steroidal surfactant with an oppositely charged thermoresponsive block copolymer, Phys. Chem. Chem. Phys. 19 (2017) 1504–1515. https://doi.org/10.1039/c6cp05665b.

[33] S. Bayati, L. Galantini, K.D. Knudsen, K. Schillén, Effects of Bile Salt Sodium Glycodeoxycholate on the Self-Assembly of PEO-PPO-PEO Triblock Copolymer P123 in Aqueous Solution, Langmuir. 31 (2015) 13519–13527. https://doi.org/10.1021/acs.langmuir.5b03828.

[34] S. Bayati, C. Anderberg Haglund, N. V. Pavel, L. Galantini, K. Schillén, Interaction between bile salt sodium glycodeoxycholate and PEO-PPO-PEO triblock copolymers in aqueous solution, RSC Adv. 6 (2016) 69313–69325. https://doi.org/10.1039/c6ra12514j.

[35] E. Tasca, A. Del Giudice, L. Galantini, K. Schillén, A.M. Giuliani, M. Giustini, A

fluorescence study of the loading and time stability of doxorubicin in sodium cholate/PEO-PPO-PEO triblock copolymer mixed micelles, J. Colloid Interface Sci. 540 (2019) 593–601. https://doi.org/10.1016/j.jcis.2019.01.075.

[36] S. Bayati, L. Galantini, K.D. Knudsen, K. Schillén, Complexes of PEO-PPO-PEO triblock copolymer P123 and bile salt sodium glycodeoxycholate in aqueous solution: A small angle X-ray and neutron scattering investigation, Colloids Surfaces A Physicochem. Eng. Asp. 504 (2016) 426–436. https://doi.org/10.1016/j.colsurfa.2016.05.096.

[37] A.J. Clulow, B. Barber, M. Salim, T. Ryan, B.J. Boyd, Synergistic and antagonistic effects of non-ionic surfactants with bile salt + phospholipid mixed micelles on the solubility of poorly water-soluble drugs, Int. J. Pharm. 588 (2020). https://doi.org/10.1016/j.ijpharm.2020.119762.

[38] M. Cárdenas, K. Schillén, V. Alfredsson, R.D. Duan, L. Nyberg, T. Arnebrant, Solubilization of sphingomyelin vesicles by addition of a bile salt, Chem. Phys. Lipids. 151 (2008) 10–17. https://doi.org/10.1016/j.chemphyslip.2007.09.002.

[39] S.J. Marrink, A.E. Mark, Molecular dynamics simulations of mixed micelles modeling human bile, Biochemistry. 41 (2002) 5375–5382. https://doi.org/10.1021/bi015613i.

[40] P. Garidel, A. Hildebrand, K. Knauf, A. Blume, Membranolytic activity of bile salts: Influence of biological membrane properties and composition, Molecules. 12 (2007) 2292–2326. https://doi.org/10.3390/12102292.

[41] C. Faustino, C. Serafim, P. Rijo, C.P. Reis, Bile acids and bile acid derivatives: use in drug delivery systems and as therapeutic agents, Expert Opin. Drug Deliv. 13 (2016) 1133–1148. https://doi.org/10.1080/17425247.2016.1178233.

[42] L. Galantini, M.C. di Gregorio, M. Gubitosi, L. Travaglini, J.V. Tato, A. Jover, F. Meijide, V.H. Soto Tellini, N. V. Pavel, Bile salts and derivatives: Rigid

unconventional amphiphiles as dispersants, carriers and superstructure building blocks, Curr. Opin. Colloid Interface Sci. 20 (2015) 170–182. https://doi.org/10.1016/j.cocis.2015.08.004.

[43] M.C. Di Gregorio, L. Travaglini, A. Del Giudice, J. Cautela, N.V. Pavel, L. Galantini, Bile Salts: Natural Surfactants and Precursors of a Broad Family of Complex Amphiphiles, Langmuir. 35 (2019) 6803–6821. https://doi.org/10.1021/acs.langmuir.8b02657.

[44] J. Cautela, B. Stenqvist, K. Schillén, D. Belić, L.K. Månsson, F. Hagemans, M. Seuss, A. Fery, J.J. Crassous, L. Galantini, Supracolloidal Atomium, ACS Nano. (2020). https://doi.org/10.1021/acsnano.0c06764.

[45] J. Cautela, V. Lattanzi, L.K. Månsson, L. Galantini, J.J. Crassous, Sphere–Tubule Superstructures through Supramolecular and Supracolloidal Assembly Pathways, Small. 14 (2018) 1–10. https://doi.org/10.1002/smll.201803215.

[46] S.C. Shin, C.W. Cho, K.H. Yang, Development of lidocaine gels for enhanced local anesthetic action, Int. J. Pharm. 287 (2004) 73–78. https://doi.org/10.1016/j.ijpharm.2004.08.012.

[47] E.H. Lee, A. Kim, Y.K. Oh, C.K. Kim, Effect of edge activators on the formation and transfection efficiency of ultradeformable liposomes, Biomaterials. 26 (2005) 205–210. https://doi.org/10.1016/j.biomaterials.2004.02.020.

[48] G. Cevc, Transfersomes, liposomes and other lipid suspensions on the skin: Permeation enhancement, vesicle penetration, and transdermal drug delivery, Crit. Rev. Ther. Drug Carrier Syst. (1996). https://doi.org/10.1615/CritRevTherDrugCarrierSyst.v13.i3-4.30.

[49] G.M. El Zaafarany, G.A.S. Awad, S.M. Holayel, N.D. Mortada, Role of edge activators and surface charge in developing ultradeformable vesicles with enhanced

skin delivery, Int. J. Pharm. 397 (2010) 164–172. https://doi.org/10.1016/j.ijpharm.2010.06.034.

[50] G.M.M. El Maghraby, A.C. Williams, B.W. Barry, Interactions of surfactants (edge activators) and skin penetration enhancers with liposomes, Int. J. Pharm. 276 (2004) 143–161. https://doi.org/10.1016/j.ijpharm.2004.02.024.

[51] Y.-K. Oh, M.Y. Kim, J.-Y. Shin, T.W. Kim, M.-O. Yun, S.J. Yang, S.S. Choi, W.-W. Jung, J.A. Kim, H.-G. Choi, Skin permeation of retinol in Tween 20-based deformable liposomes: in-vitro evaluation in human skin and keratinocyte models, J. Pharm. Pharmacol. 58 (2006) 161–166. https://doi.org/10.1211/jpp.58.2.0002.

[52] A. Sadeghpour, M. Rappolt, S. Misra, C. V. Kulkarni, Bile Salts Caught in the Act: From Emulsification to Nanostructural Reorganization of Lipid Self-Assemblies, Langmuir. 34 (2018) 13626–13637. https://doi.org/10.1021/acs.langmuir.8b02343.

[53] L. Wu, Q.L. Zhang, X.Y. Zhang, C. Lv, J. Li, Y. Yuan, F.X. Yin, Pharmacokinetics and blood-brain barrier penetration of (+)-Catechin and (-)-Epicatechin in rats by microdialysis sampling coupled to high-performance liquid chromatography with chemiluminescence detection, J. Agric. Food Chem. 60 (2012) 9377–9383. https://doi.org/10.1021/jf301787f.

[54] C. Ramassamy, Emerging role of polyphenolic compounds in the treatment of neurodegenerative diseases: A review of their intracellular targets, Eur. J. Pharmacol. 545 (2006) 51–64. https://doi.org/10.1016/j.ejphar.2006.06.025.

[55] Y.H. Lin, M.J. Tsai, Y.P. Fang, Y.S. Fu, Y. Bin Huang, P.C. Wu, Microemulsion formulation design and evaluation for hydrophobic compound: Catechin topical application, Colloids Surfaces B Biointerfaces. 161 (2018) 121–128. https://doi.org/10.1016/j.colsurfb.2017.10.015.

[56] R.K. Harwansh, P.K. Mukherjee, A. Kar, S. Bahadur, N.A. Al-Dhabi, V.

Duraipandiyan, Enhancement of photoprotection potential of catechin loaded nanoemulsion gel against UVA induced oxidative stress, J. Photochem. Photobiol. B Biol. 160 (2016) 318–329. https://doi.org/10.1016/j.jphotobiol.2016.03.026.

[57] Y. Cai, N.D. Anavy, H.H. Sherry Chow, Contribution of presystemic hepatic extraction to the low oral bioavailability of green tea catechins in rats, Drug Metab. Dispos. 30 (2002) 1246–1249. https://doi.org/10.1124/dmd.30.11.1246.

[58] K.P. Meena, M.R. Vijayakumar, P.S. Dwibedy, Catechin-loaded Eudragit microparticles for the management of diabetes: formulation, characterization and in vivo evaluation of antidiabetic efficacy, J. Microencapsul. 34 (2017) 342–350. https://doi.org/10.1080/02652048.2017.1337248.

[59] Q. Song, D. Li, Y. Zhou, J. Yang, W. Yang, G. Zhou, J. Wen, Enhanced uptake and transport of (+)-catechin and (-)-epigallocatechin gallate in niosomal formulation by human intestinal caco-2 cells, Int. J. Nanomedicine. 9 (2014) 2157–2165. https://doi.org/10.2147/IJN.S59331.

[60] J. Janiak, S. Bayati, L. Galantini, N. V. Pavel, K. Schillén, Nanoparticles with a bicontinuous cubic internal structure formed by cationic and non-ionic surfactants and an anionic polyelectrolyte, Langmuir. 28 (2012) 16536–16546. https://doi.org/10.1021/la303938k.

[61] C. V. Kulkarni, W. Wachter, G. Iglesias-Salto, S. Engelskirchen, S. Ahualli, Monoolein: A magic lipid?, Phys. Chem. Chem. Phys. 13 (2011) 3004–3021. https://doi.org/10.1039/c0cp01539c.

[62] L.M. de Buy Wenniger, T. Pusl, U. Beuers, Bile Salts, 2nd ed., Elsevier Inc., 2013. https://doi.org/10.1016/B978-0-12-378630-2.00031-1.

[63] M. Nakano, A. Sugita, H. Matsuoka, T. Handa, Small-angle X-ray scattering and 13C NMR investigation on the internal structure of “cubosomes,” Langmuir. 17 (2001)

3917–3922. https://doi.org/10.1021/la010224a.

[64] V. Meli, C. Caltagirone, C. Sinico, F. Lai, A.M. Falchi, M. Monduzzi, M. Obiols-Rabasa, G. Picci, A. Rosa, J. Schmidt, Y. Talmon, S. Murgia, Theranostic hexosomes for cancer treatments: an in vitro study, New J. Chem. 41 (2017) 1558–1565. https://doi.org/10.1039/c6nj03232j.

[65] C. Caltagirone, M. Arca, A.M. Falchi, V. Lippolis, V. Meli, M. Monduzzi, T. Nylander, A. Rosa, J. Schmidt, Y. Talmon, S. Murgia, Solvatochromic fluorescent BODIPY derivative as imaging agent in camptothecin loaded hexosomes for possible theranostic applications, RSC Adv. 5 (2015) 23443–23449. https://doi.org/10.1039/c5ra01025j.

[66] Y.K. Song, C.K. Kim, Topical delivery of low-molecular-weight heparin with surface-charged flexible liposomes, Biomaterials. 27 (2006) 271–280. https://doi.org/10.1016/j.biomaterials.2005.05.097.

[67] A. Hussain, A. Samad, M. Ramzan, M.N. Ahsan, Z. Ur Rehman, F.J. Ahmad, Elastic liposome-based gel for topical delivery of 5-fluorouracil: in vitro and in vivo investigation, Drug Deliv. 23 (2016) 1115–1129. https://doi.org/10.3109/10717544.2014.976891.

[68] S. Doppalapudi, A. Jain, D.K. Chopra, W. Khan, Psoralen loaded liposomal nanocarriers for improved skin penetration and efficacy of topical PUVA in psoriasis, Eur. J. Pharm. Sci. 96 (2017) 515–529. https://doi.org/10.1016/j.ejps.2016.10.025.